Tuning the Magnetic Anisotropy of Lanthanides on a Metal Substrate by Metal–Organic Coordination

Sofia O. Parreiras,* Daniel Moreno, Borja Cirera, Miguel A. Valbuena, José I. Urgel, Markos Paradinas, Mirco Panighel, Fernando Ajejas, Miguel A. Niño, José M. Gallego, Manuel Valvidares, Pierluigi Gargiani, Wolfgang Kuch, José I. Martínez, Aitor Mugarza, Julio Camarero, Rodolfo Miranda, Paolo Perna,* and David Écija*

Taming the magnetic anisotropy of lanthanides through coordination environments is crucial to take advantage of the lanthanides properties in thermally robust nanomaterials. In this work, the electronic and magnetic properties of Dy-carboxylate metal–organic networks on Cu(111) based on an eightfold coordination between Dy and ditopic linkers are inspected. This surface science study based on scanning probe microscopy and X-ray magnetic circular dichroism, complemented with density functional theory and multiplet calculations, reveals that the magnetic anisotropy landscape of the system is complex. Surface-supported metal–organic coordination is able to induce a change in the orientation of the easy magnetization axis of the Dy coordinative centers as compared to isolated Dy atoms and Dy clusters, and significantly increases the magnetic anisotropy. Surprisingly, Dy atoms coordinated in the metallosupramolecular networks display a nearly in-plane easy magnetization axis despite the out-of-plane symmetry axis of the coordinative molecular lattice. Multiplet calculations highlight the decisive role of the metal–organic coordination, revealing that the tilted orientation is the result of a very delicate balance between the interaction of Dy with O atoms and the precise geometry of the crystal field. This study opens new avenues to tailor the magnetic anisotropy and magnetic moments of lanthanide elements on surfaces.

1. Introduction

Lanthanide metals are nowadays ubiquitous in technology, being used in diverse fields including alloys, permanent magnets, optical fibers, luminescent devices and probes, high-temperature superconductors, and catalysts.[1–3] In addition, recent findings have highlighted the potential of lanthanides in single atom magnetism.[4,5] Fundamental requirements for a single atom magnet are: i) a doubly degenerate ground state with a high magnetic moment and ii) protection from scattering with electrons/phonons of the substrate and from quantum tunneling, which ensures the bistability of the ground state.[6] In quantum systems the stability of the magnetic moment is determined by the energy difference between the bistable ground state and the first excited state.[6] A large separation between these states protects the system against quantum fluctuations. For lanthanides, the intrinsic

Dr. S. O. Parreiras, D. Moreno, Dr. B. Cirera, Dr. M. A. Valbuena,
Dr. J. I. Urgel, Dr. F. Ajejas, Dr. M. A. Niño, Dr. J. M. Gallego,
Prof. J. Camarero, Prof. R. Miranda, Dr. P. Perna, Prof. D. Écija
Instituto Madrileño de Estudios Avanzados en Nanociencia
(IMDEA Nanociencia)
Madrid 28049, Spain
E-mail: sofia.oliveira@imdea.org; paolo.perna@imdea.org;
david.ecija@imdea.org
Dr. M. A. Valbuena, Dr. M. Paradinas, Dr. M. Panighel, Prof. A. Mugarza
Catalan Institute of Nanoscience and Nanotechnology (ICN2)
CSIC and The Barcelona Institute of Science and Technology
Campus UAB, Bellaterra, Barcelona 08193, Spain

The ORCID identification number(s) for the author(s) of this article can be found under https://doi.org/10.1002/smll.202102753.

Dr. J. M. Gallego, Dr. J. I. Martínez
Instituto de Ciencia de Materiales de Madrid (ICMM-CSIC)
Cantoblanco, Madrid 28049, Spain
Dr. M. Valvidares, Dr. P. Gargiani
ALBA Synchrotron Light Source
Barcelona 08290, Spain
Prof. W. Kuch
Institut für Experimentalphysik
Freie Universität Berlin
Arnimallee 14, 14195 Berlin, Germany
Prof. A. Mugarza
Institució Catalana de Recerca i Estudis Avançats (ICREA)
Barcelona 08010, Spain
Prof. J. Camarero, Prof. R. Miranda
Departamento de Física de la Materia Condensada and Condensed
Matter Physics Center (IFIMAC)
Universidad Autónoma de Madrid
Cantoblanco, Madrid 28049, Spain

**ADVANCED
SCIENCE NEWS**
www.advancedsciencenews.com

**NANO · MICRO
small**
www.small-journal.com

spin–orbit interaction leads to a large energy splitting between the quantum states. Furthermore, the strong localization of the 4f states reduces the hybridization with the surface, increasing the spin lifetimes,[6–8] which is crucial, since a long magnetic relaxation time is mandatory for technological applications.[4]

In this context, the stabilization of magnetic remanence in single holmium (Ho) atoms on MgO(100)/Ag(100) surfaces, with relaxation times up to 1500 s at 10 K, confirmed the feasibility of using lanthanides as single atom magnets.[4] The subsequent demonstration of electrical reading and writing of single magnetic atoms by means of electron spin resonance has experimentally proven that their use for magnetic storage is possible.[5] However, the low thermal stability, below the boiling point of nitrogen, of single standing atoms due to their high diffusion on surfaces avoids their use in practical applications. A tentative chemical strategy to increase their thermal stability could be the coordination of mononuclear lanthanide atoms in metal–organic networks. Notably, regarding single atom magnetism, lanthanides offer additional advantages over other elements. In 4f elements, the spin–orbit coupling (SOC) is larger than the crystal field (CF), which might result in higher anisotropies.[8,9] Furthermore, the CF acts as a perturbation of the SOC and can be tailored to increase the anisotropy by choosing an appropriate coordination environment,[7,10] though so far such finding has not been demonstrated for surface-confined metal–organic networks embedding lanthanides.

Contemporarily to the development of lanthanide science and technology, supramolecular chemistry on surfaces, mostly employing transition metals, has allowed the design of interfacial metal–organic complexes and architectures.[11,12] Only recently, surface-confined lanthanide-directed architectures have been reported,[3,13–18] exhibiting the affinity of lanthanides to coordinate with carbonitrile, carboxylic, and terpyridine functional groups.[19] These findings afforded the formation of lanthanide-directed networks on surfaces, which might be used to study the promising properties of f-block elements for nanomagnetism in an ordered and thermally stable coordination environment. Hereby, carboxylate-directed networks were recently reported to be stable up to 360 K.[14]

In a previous work, we have observed by X-ray photoelectron spectroscopy (XPS) a +3 oxidation state for dysprosium (Dy) atoms coordinated with linkers equipped with terminal carboxylate functional groups, namely p-terphenyl-4,4′-dicarboxylic acid (TDA) and benzene-1,4-dicarboxylic acid (TPA), on Cu(111).[13] With an odd number of electrons, Dy^{3+} is a Kramers ion with a doubly degenerate ground state,[7] fulfilling one of the prerequisites for single atom magnets. In this case, the magnetic anisotropy can be increased by a proper ligand field.[7,20] For TDA and TPA, the planar structure of the networks combined with the eightfold coordination of the Dy atoms with the oxygen atoms of the carboxylic groups is expected to result in a compressed square antiprism CF, similar to that of the {Pc(OEt)$_8$}$_2$Dy complex, where a large magnetic remanence is observed.[20]

Here we report the formation of metal–organic networks on Cu(111) based on Dy employing the two above-mentioned molecular species, TDA and TPA, in order to tailor the internodal distance while keeping a similar coordination environment. Based on a scanning probe microscopy study, combined with X-ray absorption spectroscopy (XAS), X-ray natural linear dichroism (XNLD), and X-ray magnetic circular dichroism (XMCD), and complemented by density functional theory (DFT) calculations, we reveal the electronic and magnetic properties of these Dy-carboxylate networks. On the one hand, our calculations show a metal–organic bond that is predominantly ionic, though a certain degree of covalence between dysprosium and the carboxylate moieties is observed by scanning tunneling spectroscopy (STS). On the other hand, such coordination scheme results in a change of the easy axis of magnetization of the Dy mononuclear center, which upon coordination is aligned nearly parallel to the surface, in opposition to the original out-of-plane easy axis reported for isolated dysprosium atoms on the same Cu(111) surface.[21] Notably, there is a large increment of the magnetic anisotropy of Dy and a reorientation of the anisotropy axis when compared to individual and non-coordinated Dy atoms, which is rationalized as a consequence of the combined effect of the interaction with the negative charges of the oxygen atoms and the coordination symmetry of the molecular CF. Thus, it is feasible to tune the magnetic anisotropy of lanthanide centers on surfaces by metal–organic coordination.

2. Results and Discussion

The sublimation of TDA and TPA species (see atomic models at **Figure 1**a,e) on a Cu(111) surface, held at 373 K to steer diffusion of the linkers and deprotonation of the functional groups,[13,14] followed by Dy deposition, leads to the formation of coordinated Dy-carboxylate metal–organic networks (see Figure 1b,f). These self-assembly patterns can only be designed on a substrate, since the role of the surface is critical, imposing the growth in 2D. Dy centers are imaged as voids due to the tip conditions in the scanning tunneling microscopy (STM) experiments, similarly as observed for Gd-TDA networks.[14] Such networks are stabilized by an eightfold Dy−O coordinative interaction, featuring internodal distances of 20.5(5) Å for TDA and 11.8(5) Å for TPA, as previously reported.[13]

Figure 1c,g shows DFT-optimized models for Dy-TDA and Dy-TPA interfacial architectures, respectively. The resulting optimized structure reveals that Dy atoms lie on hollow sites for both lattices. The linkers are bonded to the Dy atoms via the carboxylate terminal groups, which alternate the torsional angle within the same molecule, as previously observed for Gd-TDA networks on Cu(111).[14] The bonding energy per TDA (TPA) molecule to the Dy/Cu surface is ≈9.84 eV (10.47 eV), which has two main contributions. On the one hand, the interaction of each molecule with the metal surface is ≈1.25 eV per TDA molecule and 1.1 eV per TPA. On the other hand, ≈2.15 eV accounts for each Dy−O bond per TDA molecule (and 2.34 eV per TPA), in agreement with the expected value for a bond of a predominant ionic nature. In the case of the TDA network, the Dy−O bonding energy is ≈0.2 eV lower than for the TPA case, see Section III, Supporting Information, for comprehensive discussion.

The coordination structures calculated by DFT resemble a distorted square antiprism (D_{4d} symmetry) with the symmetry axis parallel to the surface normal. This structure was analyzed by a continuous shape measurement (CShMs),[22] as described in Section IV, Supporting Information, to determine the
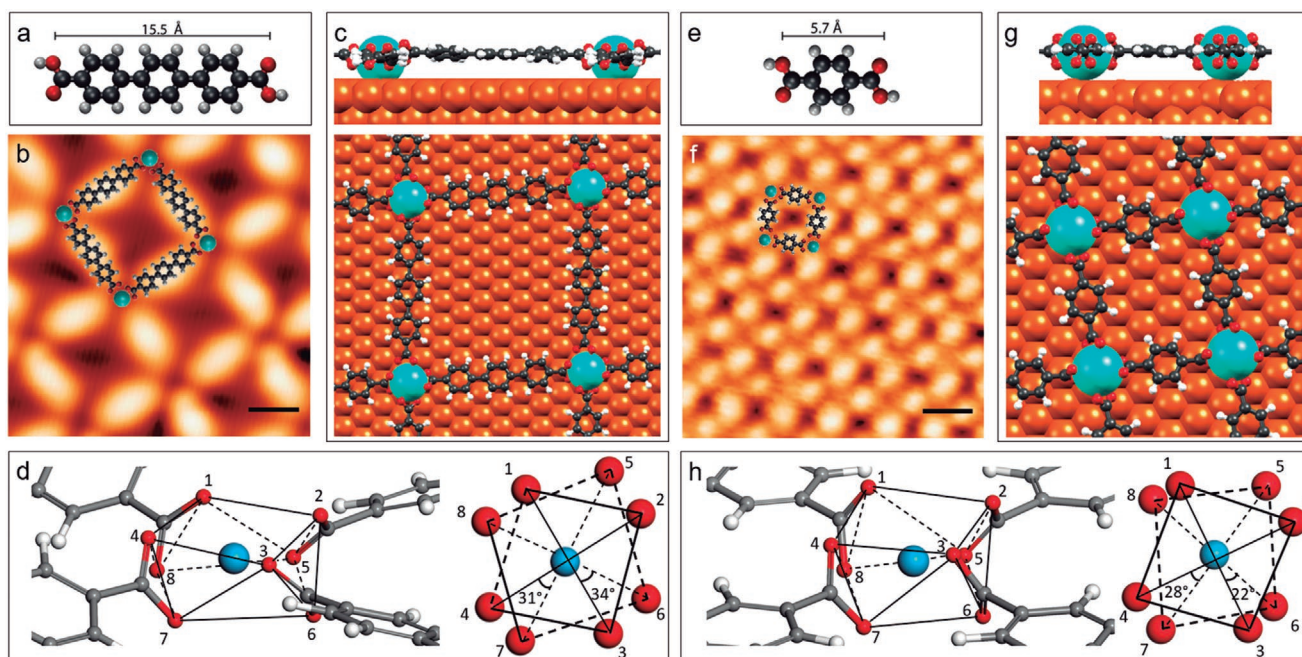
Figure 1. On-surface design of Dy-carboxylate metal–organic networks on Cu(111). a–d) Dy-TDA on Cu(111): a) Atomic model of TDA molecule where C, H, and O atoms are represented by black, white, and red balls, respectively. The indicated distance is measured between the terminal oxygen atoms. b) STM image with atomistic model superimposed. Scanning parameters: $V_b = -0.80$ V and $I = 150$ pA, $T = 4$ K, scale bar: 1.0 nm. c) Pictorial views of the DFT-optimized network. d) 3D and top views of the Dy−O coordination polyhedron. e–h) Dy-TPA on Cu(111): e) Atomic model of TPA molecule where C, H, and O atoms are represented by black, white, and red balls, respectively. The indicated distance is measured between the terminal oxygen atoms. f) STM image with atomistic model superimposed. Scanning parameters: $V_b = -1.10$ V and $I = 170$ pA, $T = 300$ K, scale bar: 1.0 nm. g) Pictorial views of the DFT-optimized network. h) 3D and top views of the Dy−O coordination polyhedron.

deviation from an ideal eightfold polyhedra. Of all symmetries allowed in the simulations, D_{4d} comes closest (see Table S1, Supporting Information, and related discussion, note that C4 is not included in the software), but with still relatively large CShMs values. This indicates that the real shapes diverge significantly from ideal D_{4d} symmetry. As expected, the antiprism is compressed in the vertical axis for both TDA and TPA lattices (Figure 1d,h). There is an additional distortion regarding the relative rotation between the two squares that deviates from the 45° of the perfect square antiprism case. The twist angles of the two diagonals are 31° and 34° (22° and 28°) for the TDA (TPA) networks. Taking into account these distortions the coordination symmetry is actually C_4.

Next, we have inspected the electronic properties of the Dy-TDA metal–organic network by means of STS, complemented with DFT calculations. To this aim we acquired point spectra on the bare substrate, uncoordinated isolated species (see explanation in Section I and Figure S1, Supporting Information), mononuclear Dy centers and coordinated molecules, as illustrated in **Figure 2**a,b. A STS spectrum measures the dI/dV signal as a function of bias voltage, which provides information on the local density of states of the sample, both at the occupied (negative bias) and unoccupied regions (positive bias), where zero bias voltage corresponds to the Fermi level. An intense resonance is found at 1.2 eV for the uncoordinated species (purple curve), whereas the coordinated one (red curve) features a strong peak at 1.7 eV, both of them assigned to the lowest unoccupied molecular orbital (LUMO) of the uncoordinated and coordinated species, respectively. No discernible

resonance is found at negative bias. A comparison with DFT simulations (Figure 2c,d) confirms our assignment of the unoccupied orbitals. The calculated projected density of states displays a LUMO resonance for the uncoordinated species (Figure 2d) that is shifted toward higher energies for the coordinated one, in qualitative agreement with the experimental results. The shift between the LUMO states upon coordination toward higher energies is visually and numerically indicated in Figure 2c,d and is attributed to a change on the adsorption geometry of the molecular species, which becomes flatter upon coordination (see Figures S5 and S6, Supporting Information). The constant current dI/dV map displays the shape of the LUMO (Figure 2f), which consists of two lobes at the rims of the molecular backbone that are more intense for molecules in one direction of the network than in another, probably due to the different registry with the substrate. Notably, spectra acquired on top of the lanthanide centers also display a resonance at similar energies as the LUMO observed for the coordinated molecular species, as depicted in the dI/dV spectrum (Figure 2a) and in the constant current map acquired at 1.6 eV (Figure 2f). This resonance is more intense in the molecular backbone and decays toward the metal center. Such finding might reveal a partial covalent nature of the coordinative Dy-carboxylate interaction.[23,24] At this stage, it is worth to point out that the metal–organic coordination based on a lanthanide bond is universally considered to be predominantly ionic, due to the internal location of the f-valence electrons, though there is always a certain degree of covalence,[2,19] which is clearly observed here for the Dy-TDA network. Our insights are
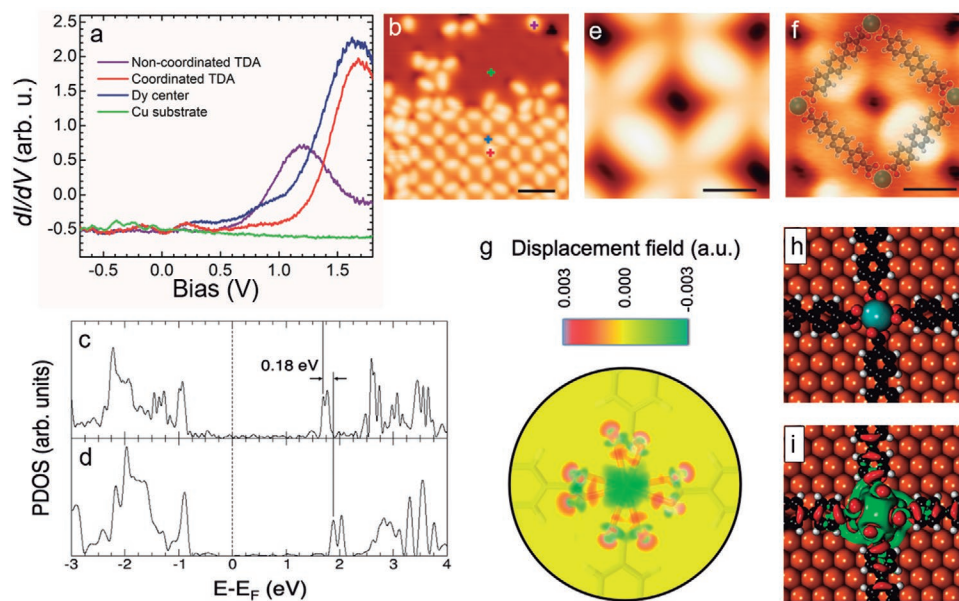
Figure 2. Electronic structure of Dy-TDA networks on Cu(111). a) STS spectra taken at coordinated TDA (red), Dy center (blue), non-coordinated TDA (purple) and Cu substrate (green). b) High-resolution STM image showing a coordinated TDA network (lower part) and non-coordinated molecules (upper part) with crosses indicating the positions where the STS spectra were taken. Scanning parameters: $V_b = -0.70$ V and $I = 80$ pA, $T = 4$ K, scale bar: 3.0 nm. c,d) Computed density of states projected onto the TDA molecule for c) non-coordinated and d) Dy-coordinated TDA/Cu(111) interfaces. e) Reference STM image for the dI/dV map. Scanning parameters: $V_b = -0.20$ V and $I = 80$ pA, $T = 4$ K scale bar: 1.0 nm. f) Constant-current dI/dV map taken at 1.60 V, showing the LUMO resonance, with a superimposed atomistic model, scale bar: 1.0 nm. g) 3D charge–density difference plot with the structural model of Dy-TDA on the Cu(111) surface superimposed. h) Top view DFT equilibrium geometry and i) isosurface corresponding to the spatially distributed 3D charge–density difference plot (with isovalues of 0.001 a.u.). Green isosurfaces represent charge depletion and red isosurfaces indicate charge accumulation.

corroborated by the calculated charge density difference plots (see Figure 2g–i and Section III, Supporting Information, for detailed analysis). The plots illustrate the difference between the electron charge density of the interacting system and those of its non-interacting counterparts. Positive values (blue, red) indicate charge accumulation, highlighting the charge gained by the carboxylate moieties. Negative values (green) represent charge depletion, and are an indication of a bond dominated by ionic interactions, in agreement with XPS data of the same network, recently published by us,[13] and in analogy to Gd-TDA networks on Cu(111).[14]

Next, we have focused our attention on the effect of molecular coordination on the electronic and magnetic properties of Dy atoms by performing XAS, XNLD, and XMCD experiments. XAS measures the X-ray absorption as a function of the incident energy, giving information on the geometric and electronic structure of the samples. This technique is element specific, allowing the identification of the chemical composition and the oxidation state. XNLD employs linearly polarized X-rays, providing fingerprints of the anisotropy of the electronic orbitals, whereas XMCD makes use of circular polarization, being the workhorse technique for inspecting the magnetic properties of the samples. Samples of Dy clusters, Dy-TDA, and Dy-TPA networks on Cu(111) were measured, maintaining a similar Dy coverage, equivalent to ≈0.01 monolayer. In addition, we compared our results to recent analogous experiments performed for isolated Dy atoms on Cu(111).[21]

Figure 3 displays XAS, XNLD, and XMCD spectra of Dy clusters and Dy centers on Dy-TDA and Dy-TPA networks taken at

the Dy $M_{4,5}$-edges at grazing (70°) and normal (0°) incidences. The spectra are presented after the subtraction of the Cu background, however XLND and XMCD spectra can be obtained directly from the raw data before the background subtraction (see Figure S4, Supporting Information). The temperature (T) of the experiments was 6 K (see the discussion of the fit of magnetization curves in Section V, Supporting Information, for more details). For Dy centers on Dy-TDA and Dy-TPA networks multiplet calculations are presented together with the experimental data and will be discussed latter.

By analyzing the peak structure of the M_5-edge, the oxidation state can be determined. The higher intensity of the third peak at 1289 eV in the XAS spectra of Dy clusters and Dy-TDA networks (Figure 3a,b) is a fingerprint of a trivalent state.[21,25] Results found in the literature for isolated Dy atoms adsorbed on Cu(111) indicate a divalent configuration,[21] and, thus, coordination with TDA changes the Dy oxidation state from +2 to +3, as typically encountered in bulk coordination chemistry.[26] The change of the oxidation state for the clusters when compared to isolated atoms is attributed to the metallic bonds between the Dy atoms, as also happens for bulk compounds.

Figure 3a,b shows XNLD spectra of Dy clusters and Dy centers on the Dy-TDA networks, respectively. XNLD was calculated as the difference between absorption spectra with linear vertical and horizontal polarizations ($\mu_V - \mu_H$) at a low magnetic field (0.01 T). The linear dichroism observed in Dy clusters reveals the anisotropy of 4f orbitals. The Dy-TDA network presents a slightly higher dichroic signal when compared to Dy clusters as a result of the CF generated by the molecular
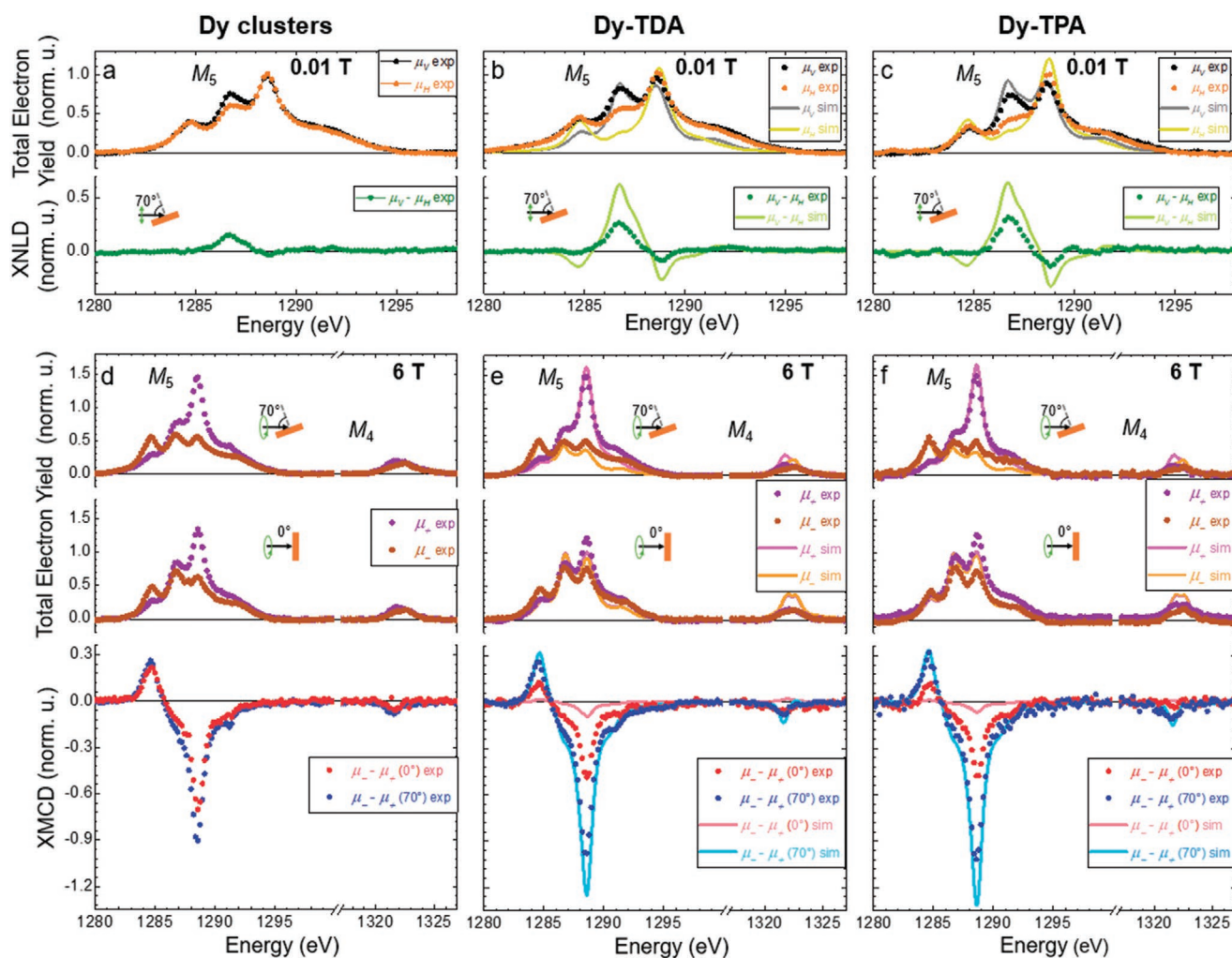
Figure 3. XAS, XNLD, and XMCD spectra of Dy clusters, Dy-TDA, and Dy-TPA networks on Cu(111). a–c) XAS spectra acquired with vertical (μ_V, black/grey spectra) and horizontal (μ_H, orange/yellow) linearly polarized light and XNLD ($\mu_V - \mu_H$, green) taken at Dy M_5-edge at grazing (70°) incidence for: a) Dy clusters, b) Dy-TDA networks, and c) Dy-TPA networks ($B = 0.01$ T, $T = 6$ K). d–f) XAS spectra acquired with positive (μ_+, purple) and negative (μ_-, brown) circularly polarized light and XMCD ($\mu_- - \mu_+$) taken at Dy $M_{4,5}$-edges at normal (0°, red) and grazing (70°, blue) incidences for: d) Dy clusters, e) Dy-TDA networks, and f) Dy-TPA networks ($B = 6$ T, $T = 6$ K). For Dy-TDA and Dy-TPA networks multiplet calculations are presented together with the experimental data.

network. These results were compared with XNLD spectra of DyPc₂ double-decker magnets,[27] which can be considered as metal–organic sandwiches of Dy with a +3 oxidation state and a D_{4d} coordination symmetry.[28] Surprisingly, such double-decker compounds show a XNLD spectrum inverted when compared to the Dy-TDA network. Even if in our case the symmetry is C_4 instead of D_{4d}, the symmetry axis has the same orientation and a similar XNLD would be expected. The inverted orientation indicates that for Dy-TDA networks the effective CF acting on the Dy atoms does not follow the coordination symmetry axis. A further comparison with Dy^{3+} ions in the dysprosium-tris(1,1,1-trifluoro-4-(2-thienyl)-2,4-butanedionate) $(Dy(tta)_3)$ complex on Au(111)[10] also confirms that the alignment of the Dy 4f orbitals in the Dy-TDA network is close to the surface plane (see the Experimental Section for more details).

Concerning the magnetic properties, isolated Dy atoms on Cu(111) at 2.5 K have been recently reported to be almost isotropic, having a very small magnetic anisotropy with an out-of-plane easy axis.[21] However, the intensity of the XMCD signal of Dy clusters on Cu(111) for grazing incidence is larger than for normal incidence (Figure 3d) revealing a change of the anisotropy axis, which proves that it is possible to tune the magnetic anisotropy of Dy by adjacent metallic bonds, as found for other lanthanide elements.[29]

In order to exploit such magnetic anisotropy, Dy-directed metal–organic architectures are ideal candidates because their mononuclear configuration imposes a specific CF to the lanthanide sphere. In fact, XMCD experiments of surface-supported Dy-TDA networks show a drastic increase of the difference between grazing and normal XMCD intensity of Dy (Figure 3e). Sum rules[30,31] were used to calculate the projections of the magnetic moments at the experimental conditions of 6 T and a temperature of 6 K (see Experimental Section) and the results for grazing (70°) and normal (0°) incidences are presented in

ADVANCED
SCIENCE NEWS
www.advancedsciencenews.com

NANO · MICRO
small
www.small-journal.com

Table 1. Expectation values at the experimental temperature and at 6 T field of orbital ($\langle L_z \rangle$), spin ($\langle S_z \rangle$) and total ($\langle J_z \rangle$) moments, total magnetic moment (M_T), and moment anisotropy (ΔM_T) obtained from XMCD sum rules for normal (0°) and grazing (70°) incidences for Dy clusters on Cu(111) and Dy centers on Dy-TDA and Dy-TPA networks on Cu(111).

	Dy clusters on Cu(111)		Dy centers on TDA network		Dy centers on TPA network		Dy single atoms on Cu(111)[21]	
Incidence angle [°]	0	70	0	70	0	70	0	60
$\langle L_z \rangle$ [ℏ]	1.19 (12)	1.87 (19)	1.36 (14)	2.35 (24)	1.00 (10)	2.77 (28)	4.7 (2)	4.4 (2)
$\langle S_z \rangle$ [ℏ]	0.65 (6)	0.86 (9)	0.44 (4)	1.14 (11)	0.60 (6)	1.18 (11)	1.6 (1)	1.5 (0)
$\langle J_z \rangle$ [ℏ]	1.84 (18)	2.73 (27)	1.80 (18)	3.49 (35)	1.60 (16)	3.95 (40)	6.3 (2)	5.9 (2)
M_T [μ_B]	2.49 (25)	3.59 (36)	2.24 (22)	4.63 (46)	2.20 (22)	5.13 (51)	7.9 (2)	7.4 (2)
ΔM_T [μ_B]	1.10 (61)		2.39 (68)		2.93 (73)		0.5 (3)	

Table 1. We define the moment anisotropy ΔM_T as the difference between grazing and normal magnetic moments measured at 6 T and 6 K ($\Delta M_T = M_T(70°) - M_T(0°)$). Data for Dy^{2+} single atoms on Cu(111) from reference [21], measured at 6.8 T and 2.5 K, is also presented for comparison.

Here it is worth mentioning that lanthanides show a high SOC and their electronic and magnetic properties are described by the quantum numbers J and J_z. On surfaces, Dy^{3+} shows a remarkably high orbital moment, as observed for other rare-earths[6,21] and contrary to 3d metals.[35] Importantly, the orbital moment is not quenched by the ligand field, being of the same order of magnitude than the spin moment. As can be seen in Table 1, both orbital and spin moments differ strongly for normal and grazing incidences. When comparing the moment anisotropies (ΔM_T) of Dy clusters on Cu(111) and Dy centers in Dy-TDA networks, the latter is 2.2 times greater, due to the cooperative effect of the CF. Furthermore, the high moment anisotropy of Dy-TDA can be clearly observed when comparing XMCD spectra acquired at 0° and 70° incidences, and the $\langle J_z \rangle$ evaluated for grazing incidence is more than twice larger than for normal incidence (Figure 3e). In the case of isolated Dy^{2+} atoms adsorbed on Cu(111), the difference between the spectra measured at 0° and 60° is negligible, and the resulting moments are very close, with a difference ≈7%.[21] Thus, the moment anisotropy of Dy^{3+} centers in Dy-TDA networks is much higher than for Dy^{2+} isolated atoms.

Figure 4a,b displays magnetization curves of Dy clusters and Dy-TDA calculated by evaluating the variation of the XMCD signal of the highest peak of the M_5-edge with the applied magnetic field. The curves were fitted to the model described in the Experimental Section. During the fits, the value of anisotropy energy (D) was going to high negative values (minus infinity), indicating strong easy-axis anisotropy, which at the temperature and for the fields used in the experiment means that the system is basically modeled by an effective spin-1/2 system, with only the ground-state doublet being significantly occupied. Additionally, fit deviation data indicates that a wider range of D values is tolerated by Dy clusters suggesting that the molecular networks may have larger anisotropy energy than the clusters (see Figure S9, Supporting Information). The similar slope of the curves obtained at grazing and normal incidences for all samples can be reproduced by easy axes tilted by 73°–65° away from the surface normal. The higher XMCD signal for grazing incidence is then explained by the larger projection of this (azimuthally averaged) easy axis onto the grazing incidence direction of the X-rays compared to the case of normal incidence.

Importantly, the very similar slope of the experimental M(H) curves for normal and grazing incidences together with the significant difference in the XMCD signal at 6 T can neither be modeled by an in-plane easy-axis anisotropy nor by an easy-plane anisotropy in the surface plane. In both cases the curvature in the hard-axis direction, for normal incidence, would be inconsistent with the experimental observation. Both results, however, can be explained by an oblique orientation of the quantization axis of the Dy ions.

As mentioned before, in the discussion of Figure 3a,b, the XNLD spectra show an intensity asymmetry compatible with 4f orbitals aligned parallel to the surface. However, it is not possible to determine if they are lying totally in-plane or are in a tilted orientation close to the surface. Considering this tilted orientation of the anisotropy axis it is possible that the 4f orbitals have also an oblique orientation following the quantization axis.

In the case of the clusters, the fitted angle of 65.0° between the quantization axis and the surface normal is attributed to the averaging of Dy atoms with distinct anisotropy orientations, since Dy was deposited at room temperature and diffused forming clusters, bulkier than their metallosupramolecular architecture counterparts.

Figure 4d presents XAS and XMCD spectra of Dy centers on Dy-TDA networks taken at a temperature of 6 K at the Dy $M_{4,5}$-edges for incidence angles ranging from 0° (normal) to 80°. The experimental angle dependence was compared with models for the easy axis oriented in-plane, out-of-plane, and in a tilted angle of 71.2° from the normal as obtained from the fitting of the magnetization curves. Figure 4e presents the experimental data of the angular variation of the integrated M_5 XMCD signal and maximum intensity together with the theoretical models. It is clear that the experimental data does not follow the expected behavior for in-plane nor for out-of-plane anisotropy, being closer to the tilted model.

It is important to point out that the magnetic moments presented in Table 1 correspond to the projections of the moments on the incidence directions (0° and 70°) at 6 T and a temperature of 6 K. To determine the saturation values, it would be necessary to measure aligning the beam to the quantization axis. However, the networks grow in domains, and given the relationship between the network unit cell and the surface high-symmetry directions, there is a total of six possible
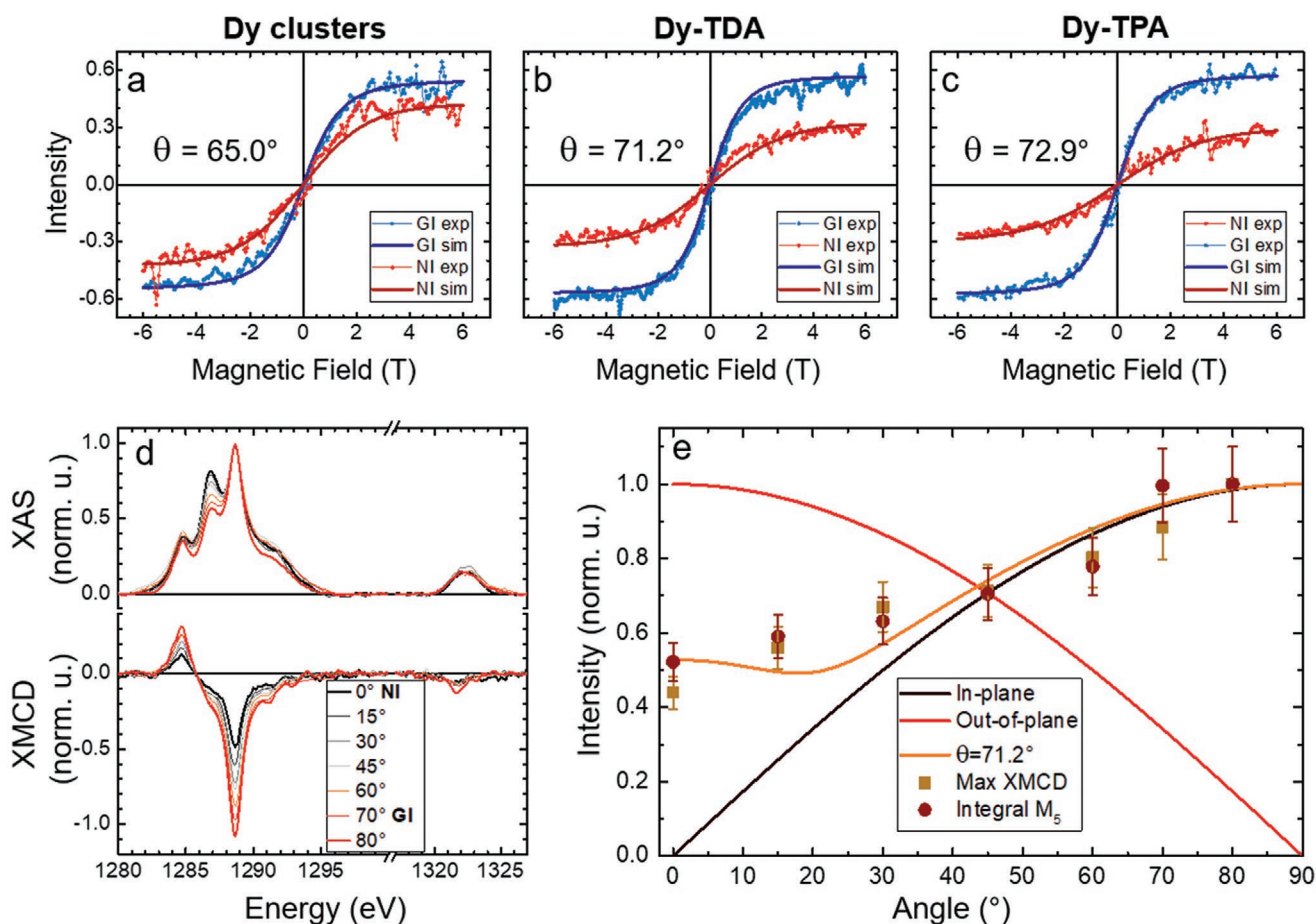
**ADVANCED
SCIENCE NEWS**

www.advancedsciencenews.com

NANO · MICRO

small

www.small-journal.com

Figure 4. Magnetization curves of Dy clusters, Dy-TDA and Dy-TPA networks on Cu(111) and angle dependence of Dy-TDA integrated XMCD. a–c) Magnetization curves acquired by measuring the intensity of the XMCD signal at the M_5-edge at the highest peak for: a) Dy clusters, b) Dy-TDA network, and c) Dy-TPA network ($T = 6$ K). The curves were fitted according to the model described in the SI ($T = 6$ K). In the y scale 1 corresponds to a full alignment of a not-azimuthally-rotated Dy magnetization with the X-ray incidence. d) XAS-TEY $\left(\frac{\mu_+ + \mu_-}{2}\right)$ and XMCD $(\mu_- - \mu_+)$ spectra taken at the Dy $M_{4,5}$-edges at incidence angles (θ) ranging from 0° (normal) to 80° (grazing) for Dy centers on Dy-TDA networks on Cu(111) ($B = 6$ T, $T = 6$ K). e) Angle dependence data for the Dy-TDA network. Dark yellow dots are the maximum intensity of the M_5-edge, wine dots are the integrated M_5 XMCD signal. The lines are some theoretical models with the easy axes oriented at distinct angles (θ) with respect to the surface plane. The simulated curves are the projection of the expectation value of the magnetization on the light incidence direction at 6 T. It was assumed that they are proportional to the maximum XMCD as well as the integrated XMCD. Both, theoretical curves and experimental data, were normalized so that 1 correspond to the maximum intensity.

orientational domains. Experimentally, what is measured is an average over these six domains and the system will never be totally saturated. Nevertheless, it is possible to have an estimate of the saturation values when dividing the moments in Table 1 by the intensities of the simulated magnetization curves at 6 T presented in Figure 4a–c.

The explanation for the origin of the tilted easy axis of magnetization is not trivial. As discussed previously, the CF imposed on Dy centers by the TDA network leads to a compressed and distorted square antiprism coordination polyhedron. The square antiprism is the coordination environment of double-decker magnets,[28] which display out-of-plane anisotropies,[27,33] following the D_{4d} symmetry axis. However, the anisotropy in lanthanide systems is very complex and can be drastically altered by minor changes in the coordination environment.[32] A recently reported system with a similar coordination symmetry

is the [Na{Dy(DOTA)(H$_2$O)}]·4H$_2$O salt (Dy-DOTA), which presents a decker plane formed by oxygen atoms apically capped with a water molecule. In this salt, the anisotropy orientation is not linked to the symmetry axis of the coordination polyhedron, but nearly orthogonal to it, that is, almost perpendicular to the one observed for double-deckers.[32,34] Moreover, theoretical calculations for the salt showed that small structural changes, such as the rotation or removal of the water molecule, leads to abrupt changes on the magnetic anisotropy. Dy-TDA networks on Cu(111) behave magnetically in a way more similar to Dy-DOTA than to double-deckers, with the easy axis of magnetization oriented in a small angle close to the surface plane.

To better understand this orientation of the easy axis we have performed a series of multiplet calculations using the MultiX code.[36] These simulations reveal that the anisotropy is the result of a delicate balance between different contributions.

On one side, the symmetry axis of the coordination polyhedron favors an out-of-plane orientation. On the other side, the interaction of the negative charges of the oxygen atoms with the positive charge of the Dy^{3+} ion changes the charge distribution, favoring an in-plane orientation. The balancing of these two opposite contributions results in a tilted easy axis. For a perfect square antiprism, the effect of the charge interaction is stronger than the coordination symmetry and the in-plane component is larger (see Figure S10, Supporting Information). The orientation of the magnetic anisotropy and the angle dependence of XMCD spectra depend on the precise geometry of the CF. The effect of distortions from the ideal D_{4d} symmetry on the XNLD and XMCD spectra is described in Section VI, Supporting Information, (see Figures S11–S13, Supporting Information, and related discussion).

A comparison between XAS, XNLD, and XMCD simulations and measurements for Dy-TDA networks is shown in Figure 3b,e. Although a perfect fit between experiment and simulation was not achieved due to the difficulty of reproducing the exact coordination symmetry of the real molecular CF, there is a reasonable qualitative agreement: the peak structure of XAS, the sign of the XNLD and the larger intensity of XMCD for grazing incidence are well reproduced. Notably, we have also explored the impact of the substrate on the magnetic properties, not finding significant contributions. The role of the Cu(111) support is to fix the coordination geometry, but beyond that important structural contribution, the magnetic properties are determined by the lanthanide-ligand field interactions (see Figure S15, Supporting Information).

Despite the changes in XMCD intensity with coordination, the magnetization curves still present a paramagnetic behavior, with no opening of the hysteresis loop and no remanence. In principle, a Dy^{3+} Kramers ion with $J = 15/2$ would imply 8 feasible doubly degenerate $|J_z|$ states, being an excellent candidate for measuring magnetic remanence, that is, behaving as single atom magnet.[4,5] The absence of single atom magnet behavior can be tentatively explained by distinct factors: the interaction of the Dy atoms i) with the metallic substrate via conduction electrons and phonon modes or ii) with the molecules via phonons could destabilize the magnetic moments;[21,37–39] iii) the magnetic relaxation time could be smaller than the measuring time, which would avoid the observation of the magnetic remanence.[25]

In an attempt to see the influence of the internodal distance on the magnetic properties of the network, we engineered a Dy-TPA metal–organic coordination network on Cu(111) where the distance between Dy centers is ≈50% shorter than in the Dy-TDA network, but featuring the same coordination environment. On one hand, the reduction of the length of the molecular precursor has been investigated as a route to reduce the vibrational excitations and limit phonon interactions, which could help to stabilize the magnetic remanence. On the other hand, it is necessary to know if there is any coupling between the lanthanide centers, which could be pernicious for stabilizing a single atom magnet, but very relevant for engineering lanthanide-based metal–organic ferromagnets.[40]

By performing XAS, it is found that the oxidation state of Dy in the Dy-TPA network is again +3 (Figure 3c). XNLD reveals that the Dy 4f orbitals in Dy-TPA networks also display a symmetry axis close to the plane (Figure 3c) and the effective CF is even larger than in the Dy-TDA counterparts (Figure 3b). This increase is attributed to the small differences in the coordination symmetry between both networks, which should also influence the magnetic properties.

Magnetic moments of Dy-TPA calculated from sum rules show larger moment anisotropy (ΔM_T in Table 1), being 2.7 times greater than the moment anisotropy of Dy clusters and 1.2 times greater than that of Dy-TDA networks (note the importance of the error bar for a rigorous comparison). Such increase in moment anisotropy can be a consequence of the differences in the coordination antiprism, since minor variations in the coordination geometry can lead to major changes in the magnetic moments. The fitting of the magnetization curves (Figure 4c) again indicates an anisotropy energy in the maximum negative limit (see Table S2, Supporting Information). The changes in the magnetization curves for the different systems are due to the reorientation of the easy axis, not to any change in the anisotropy energy. For Dy-TPA, the easy axis of magnetization is oriented at a smaller angle when compared to Dy-TDA, closer to the surface plane, 72.9° from the surface normal. The smaller tilting angle of the easy axis is attributed to differences in the geometry of the CF, as predicted by DFT and multiplet calculations. The coordination polyhedron of Dy-TPA has a lower compression and a higher twist angle between the oxygen planes than that of Dy-TDA. According to multiplet calculations, both changes contribute to increase the difference between grazing and normal XMCD intensity (see Figures S12 and S13, Supporting Information, and related discussion). A comparison between simulations and experimental XAS, XNLD and XMCD spectra for Dy-TPA is shown in Figure 3c,f. Similar to Dy-TDA, there is a good qualitative agreement with the experimental results and the role of the Cu(111) substrate is negligible (see Figure S16, Supporting Information).

Although the magnetization curves still exhibit a paramagnetic behavior, the change of the molecular linker improved the magnetic properties. The high magnetic anisotropy is preserved and the projected magnetic moments are even larger, as can be seen in Table 1. Our findings demonstrate that these Dy-directed metal–organic networks are very robust and suitable for tuning the magnetic anisotropy of lanthanides and, thus, opening avenues in the development of single atom magnetism. A promising approach to further advance and stabilize the magnetic remanence is the insertion of decoupling layers between the substrate and the molecular network. Graphene, MgO, and other insulating layers have been demonstrated to be effective on decoupling lanthanides from metallic substrates.[4,41,42] Graphene was also used to decouple Co metal–organic networks from an iridium substrate.[23,43] Furthermore, long relaxation times have been observed for Dy single atoms adsorbed on graphene/Ir(111),[37] revealing a promising substrate for the preparation of coordinated Dy networks.

3. Conclusion

In summary, we have studied the electronic and magnetic properties of Dy-carboxylate metal–organic networks on Cu(111)

using two ditopic linkers, TDA and TPA, featuring distinct internodal distances, but a similar coordination environment.

Regarding the electronic properties, the coordination is dominated by ionic interactions with a minority covalent component. Dysprosium coordinative centers feature a +3 oxidation state, underlining that it is feasible to tailor the oxidation state of lanthanides on surfaces by metal–organic coordination. For both networks, the symmetry axis of Dy 4f orbitals is close to the surface.

Concerning magnetism, the easy axis of magnetization was found to be lying nearly in-plane, despite the out-of-plane orientation of the coordination symmetry axis. Such a finding highlights the complexity of the magnetism of lanthanide systems on surfaces, which can be drastically affected by small structural changes due to molecular coordination and by interaction with the charges of coordination linkers. The magnetic properties are the result of a delicate balance between the interaction of Dy^{3+} with the negative charges of oxygen atoms and the precise geometry of the CF. Subtle changes in the coordination symmetry of Dy-TPA when compared to Dy-TDA lead to a change in the tilting angle of the anisotropy axis, which is slightly smaller for Dy-TPA. Dy^{3+} centers in Dy-TDA and Dy-TPA networks have stronger magnetic anisotropies than isolated Dy^{2+} atoms and higher magnetic moments than Dy^{2+} atoms or Dy^{3+} clusters. However, it was not possible to observe any magnetic remanence, which is attributed to either short spin relaxation time or scattering with conduction electrons and phonon modes arising from the molecular or metallic environment.

Since we show that it is feasible to tame the magnetic anisotropy of lanthanides by coordinative protocols, we propose to grow such metal–organic architectures on non-conductive layers or ultra-thin film insulators as a paradigm to stabilize the magnetic remanence by reducing the interaction with the substrate. In this quest, networks should be carefully designed to allow enough internodal distances to prevent coupling of lanthanide centers.

4. Experimental Section

Experimental Methods: The Cu(111) substrate was prepared by cycles of sputtering (Ar+, 800 eV) and annealing (723 K, 10 min). TDA and TPA molecules (purchased from Sigma-Aldrich) were deposited by organic molecular deposition from Knudsen cells (Kentax evaporator) on the clean Cu surface (see Figure S2, Supporting Information) heated to 373 K. Next, Dy was deposited by e-beam evaporation from a metal rod (Omicron 3-cell evaporator) with the substrate still maintained at 373 K. Dy clusters were prepared by the deposition of an amount of Dy similar to the one used in the networks (≈0.01 monolayer) directly on the clean Cu surface at room temperature (300 K). All the experiments were carried out in situ in UHV chambers with base pressures below 5×10^{-10} mbar. STM experiments were done in two different systems. TPA networks were measured with an Aarhus-150 VT-STM at room temperature. TDA networks were analyzed in an Omicron LT-STM at 4 K. In both cases, the images were taken using tungsten tips and measured in constant current mode. dI/dV spectroscopy was acquired by stabilizing the tip, opening the feed-back loop, applying a V_{bias} ramp with a modulation of 10 meV and recording the dI/dV signal with a lock-in amplifier.

For the synchrotron experiments the samples were prepared with an excess of molecules to ensure that all Dy atoms are coordinated with molecules and no magnetic signal is arising from Dy clusters and/or uncoordinated single atoms. Such behavior was checked by STM experiments carried out with an Aarhus-150 VT-STM at room temperature, where large domains of coordinated network in coexistence with uncoordinated molecules were observed. Notably the absence of Dy clusters was also corroborated. Figure S3, Supporting Information, presents large scale images of the Dy-TDA network. The same preparation procedure was also followed for Dy-TPA networks, guaranteeing that all Dy atoms are coordinated.

XAS, XNLD, and XMCD measurements were performed at the BOREAS beamline of the ALBA synchrotron light source, Spain. The experiments have been done in total electron yield (TEY) mode with a 90% circularly polarized beam and magnetic fields up to 6 T. The nominal temperature was 2 K, however, as is discussed in Section V, Supporting Information, the fitting of the magnetization curves indicates that the real temperature is higher, ≈6 K. For a matter of clarity, only the fitting temperature is indicated in the main text. XNLD is the difference between spectra measured with vertical and horizontal polarizations ($\mu_V - \mu_H$). The spectra were measured at 0.01 T and normalized at the Dy M_5-edge of isotropic spectra: $Iso_{XNLD} = \left(\frac{1}{3}\mu_V + \frac{2}{3}\mu_H\right)$. XAS spectra were obtained from the average of the spectra measured with two circular polarizations $\left(\frac{\mu_+ + \mu_-}{2}\right)$. XMCD is the difference between negative and positive polarizations ($\mu_- - \mu_+$). XAS and XMCD spectra were normalized by the Dy M_5-edge of average absorption spectra: $Ave_{XAS} = \left(\frac{\mu_+ + \mu_-}{2}\right)$.

Figure S4, Supporting Information, shows XAS and XMCD spectra of the Dy-TDA network on Cu(111) taken at the Dy $M_{4,5}$-edges acquired with positive (μ_+) and negative (μ_-) circularly polarized light. The figure presents the raw data before background subtraction (Figure S4a, Supporting Information) as also the normalized spectra after background subtraction (Figure S4b, Supporting Information). The XMCD spectrum in Figure S4a, Supporting Information, was obtained by the difference between XAS spectra with negative and positive polarization before the background subtraction. STM was used to provide information on the morphology of the metal–organic network as well as to calibrate the coverage.

When comparing XNLD spectra with results found in the literature, it is necessary to take into account how the spectra were defined. Studniarek et al.[27] defined the XNLD as ($\mu_V - \mu_H$), which allows a direct comparison with our spectra. On the other side, in the work of Stoll et al.[10] it is defined as ($\mu_{25°} - \mu_{90°}$); considering that $\mu_\theta = [\cos(\theta)]^2 \cdot \mu_V + [\sin(\theta)]^2 \cdot \mu_H$ (see supplementary note 6 of ref. [44]), this implies that ($\mu_{25°} - \mu_{90°}$) = $0.18 \cdot (\mu_H - \mu_V)$. As only the spectral shapes are being compared, not the intensities, the proportionality factor is not relevant and it is only necessary to invert the spectra to have ($\mu_V - \mu_H$) and compare with our XLND results. After the inversion, our spectra have the same orientation as the Dy^{3+} ions in the dysprosium-tris(1,1,1-trifluoro-4-(2-thienyl)-2,4-butanedione) (Dy(tta)$_3$) complex on Au(111), where the symmetry axis of 4f orbitals is lying in-plane. As discussed in the main text, for our systems it is possible that the symmetry axis is the same as the anisotropy quantization axis, presenting a tilted orientation close to the plane, but it is not possible to determine undoubtedly this orientation. The XNLD spectra only indicate that the symmetry axis is closer to the surface plane.

Expectation values of orbital $\langle L_z \rangle$ and effective spin $\langle S_{zeff} \rangle = \langle S_z \rangle + 3\langle T_z \rangle$ moments in units of $\hbar$ were calculated using sum rules[30,31] with the quantum numbers $c = 2$ and $l = 3$, and the number of holes $n_H = 5$ for Dy^{3+}.[45] The spin moment $\langle S_z \rangle$ was separated from the dipole contribution $\langle T_z \rangle$ assuming the theoretical value $\frac{\langle T_z \rangle}{\langle S_z \rangle} = -0.053$ for Dy^{3+}.[46] The total magnetic moment per atom was also calculated in μ_B, $M_T = 2\langle S_z \rangle + \langle L_z \rangle$. The moment anisotropy of M_T is defined in this work as the difference between the projections of the magnetic moments on the incidence direction at grazing and normal incidences in a field of 6 T and a temperature of 6 K, $\Delta M_T = M_T (70°) - M_T (0°)$.

Theoretical Framework and Computational Details: Ab initio calculations for structural optimization and electronic structure properties have been carried out by DFT as implemented in the plane-wave QUANTUM

ESPRESSO simulation package.[47] One-electron wave-functions were expanded in a plane-waves basis with energy cutoffs of 500 and 600 eV for the kinetic energy and the electronic density, respectively. Exchange and correlation have been computed in the revised generalized gradient corrected approximation PBESol.[48,49] Kresse–Joubert projector augmented wave pseudopotentials[50] have been adopted to model the ion–electron interaction for all the involved atoms (H, C, O, Cu, and Dy) in order to include the SOC effect and a potential non-collinearity of spins. Besides, 20 valence electrons have been accounted for the Dy atom in order to check the role of the lanthanide $4f^{10}$ electrons in the subtle interfacial chemistry. In all the calculations, Brillouin zones have been sampled using optimal Monkhorst–Pack grids ($2 \times 2 \times 1$) during structural relaxation and $4 \times 4 \times 1$ for the electronic calculation).[51] A perturbative van der Waals (vdW) correction, with an empirical vdW R-6 correction, was used to add dispersive forces to conventional density functionals (DFT+D3).[52] Atomic relaxations were carried out using a conjugate gradient minimization scheme until the maximum force on any atom was lower than 0.02 eV Å^{-1}. The Fermi level was smeared out using the Methfessel–Paxton approach[53] with a Gaussian width of 0.01 eV, and all energies were extrapolated to $T = 0$ K. Self-consistency in the electron density was converged to a precision in the total energy better than 10^{-6} eV.

Theoretical Fit of Magnetization Curves: The theoretical model uses a simple spin Hamiltonian with uniaxial zero-field splitting characterized by the axial zero-field splitting parameter D: $H = \mu_B g_J \vec{B} \cdot \vec{J} + D J_z^2$, where we use $J = 15/2$ and the Landau g factor $g_J = 4/3$ for the nine $4f$ electrons of Dy^{3+}. To simulate the field-dependent XMCD we neglect the dipole term of the magnetic moment, T_z, which is expected to be small for Dy[46] and populate the eigenstates of H thermally according to the temperature T. The quantization axis is oriented under a fixed polar angle θ defined with respect to the surface normal. To account for random azimuthal orientations of the structures on the surface, we perform an azimuthal averaging over all orientations of the easy axis rotated around the surface normal for the same polar angle theta. Details of the procedure are described in reference [10].

Multiplet Calculations: The calculations have been done using the MultiX code,[36] for a Dy^{3+} ion with $3d^{10}4f^9$ ground state, a temperature of 6 K (as determined by the fitting of magnetization curves), and magnetic fields of 6 T for XMCD and 0.01 T for XNLD. The Hartree–Fock parameters where rescaled by factors of 0.96 for the SOC and 0.80 for the Coulomb interaction and a core–hole broadening of 0.5 eV was used to reproduce the experimental resolution. The CF was simulated using point charges, that is, the coordinates and charges of the neighboring atoms were used to simulate their interaction with Dy.

Supporting Information

Supporting Information is available from the Wiley Online Library or from the author.

Conflict of Interest

The authors declare no conflict of interest.

Data Availability Statement

Research data are not shared.

[1] S. V. Eliseeva, J. -C. G. Bünzli, *New J. Chem.* **2011**, *35*, 1165.

[2] J. -C. G. Bünzli, *J. Coord. Chem.* **2014**, *67*, 3706.

[3] D. Écija, J. I. Urgel, A. P. Seitsonen, W. Auwärter, J. V. Barth, *Acc. Chem. Res.* **2018**, *51*, 365.

[4] F. Donati, S. Rusponi, S. Stepanow, C. Wäckerlin, A. Singha, L. Persichetti, R. Baltic, K. Diller, F. Patthey, E. Fernandes, J. Dreiser, Ž. Šljivančanin, K. Kummer, C. Nistor, P. Gambardella, H. Brune, *Science* **2016**, *352*, 318.

[5] F. D. Natterer, K. Yang, W. Paul, P. Willke, T. Choi, T. Greber, A. J. Heinrich, C. P. Lutz, *Nature* **2017**, *543*, 226.

[6] F. Donati, A. Singha, S. Stepanow, C. Wäckerlin, J. Dreiser, P. Gambardella, S. Rusponi, H. Brune, *Phys. Rev. Lett.* **2014**, *113*, 237201.

[7] J. D. Rinehart, J. R. Long, *Chem. Sci.* **2011**, *2*, 2078.

[8] T. Schuh, T. Miyamachi, S. Gerstl, M. Geilhufe, M. Hoffmann, S. Ostanin, W. Hergert, A. Ernst, W. Wulfhekel, *Nano Lett.* **2012**, *12*, 4805.

[9] S. T. Liddle, J. van Slageren, *Chem. Soc. Rev.* **2015**, *44*, 6655.

[10] P. Stoll, M. Bernien, D. Rolf, F. Nickel, Q. Xu, C. Hartmann, T. R. Umbach, J. Kopprasch, J. N. Ladenthin, E. Schierle, E. Weschke, C. Czekelius, W. Kuch, K. J. Franke, *Phys. Rev. B* **2016**, *94*, 224426.

[11] J. V. Barth, *Annu. Rev. Phys. Chem.* **2007**, *58*, 375.

[12] L. Dong, Z. Gao, N. Lin, *Prog. Surf. Sci.* **2016**, *91*, 101.

[13] B. Cirera, L. Dordevic, R. Otero, J. M. Gallego, D. Bonifazi, R. Miranda, D. Ecija, *Chem. Commun.* **2016**, *52*, 11227.

[14] J. I. Urgel, B. Cirera, Y. Wang, W. Auwärter, R. Otero, J. M. Gallego, M. Alcamí, S. Klyatskaya, M. Ruben, F. Martín, R. Miranda, D. Ecija, J. V. Barth, *Small* **2015**, *11*, 6358.

[15] J. I. Urgel, D. Ecija, W. Auwärter, D. Stassen, D. Bonifazi, J. V. Barth, *Angew. Chem., Int. Ed.* **2015**, *54*, 6163.

[16] D. Écija, J. I. Urgel, A. C. Papageorgiou, S. Joshi, W. Auwärter, A. P. Seitsonen, S. Klyatskaya, M. Ruben, S. Fischer, S. Vijayaraghavan, J. Reichert, J. V. Barth, *Proc. Natl. Acad. Sci. U. S. A.* **2013**, *110*, 6678.

[17] J. I. Urgel, D. Écija, G. Lyu, R. Zhang, C. -A. Palma, W. Auwärter, N. Lin, J. V. Barth, *Nat. Chem.* **2016**, *8*, 657.

[18] G. Lyu, Q. Zhang, J. I. Urgel, G. Kuang, W. Auwärter, D. Ecija, J. V. Barth, N. Lin, *Chem. Commun.* **2016**, *52*, 1618.

[19] J. -C. G. Bünzli, *Acc. Chem. Res.* **2006**, *39*, 53.

[20] N. Ishikawa, Y. Mizuno, S. Takamatsu, T. Ishikawa, S. Koshihara, *Inorg. Chem.* **2008**, *47*, 10217.

[21] A. Singha, R. Baltic, F. Donati, C. Wäckerlin, J. Dreiser, L. Persichetti, S. Stepanow, P. Gambardella, S. Rusponi, H. Brune, *Phys. Rev. B* **2017**, *96*, 224418.

[22] D. Casanova, M. Llunell, P. Alemany, S. Alvarez, *Chem. - Eur. J.* **2005**, *11*, 1479.

[23] A. Kumar, K. Banerjee, A. S. Foster, P. Liljeroth, *Nano Lett.* **2018**, *18*, 5596.

[24] J. Li, L. Solianyk, N. Schmidt, B. Baker, S. Gottardi, J. C. M. Lopez, M. Enache, L. Monjas, R. van der Vlag, R. W. A. Havenith, A. K. H. Hirsch, M. Stöhr, *J. Phys. Chem. C* **2019**, *123*, 12730.

[25] R. Baltic, F. Donati, A. Singha, C. Wäckerlin, J. Dreiser, B. Delley, M. Pivetta, S. Rusponi, H. Brune, *Phys. Rev. B* **2018**, *98*, 024412.

[26] M. N. Bochkarev, *Coord. Chem. Rev.* **2004**, *248*, 835.

[27] M. Studniarek, C. Wäckerlin, A. Singha, R. Baltic, K. Diller, F. Donati, S. Rusponi, H. Brune, Y. Lan, S. Klyatskaya, M. Ruben, A. P. Seitsonen, J. Dreiser, *Adv. Sci.* **2019**, *6*, 1901736.

[28] H. Wang, K. Wang, J. Tao, J. Jiang, *Chem. Commun.* **2012**, *48*, 2973.

[29] A. Singha, F. Donati, C. Wäckerlin, R. Baltic, J. Dreiser, M. Pivetta, S. Rusponi, H. Brune, *Nano Lett.* **2016**, *16*, 3475.

[30] B. T. Thole, P. Carra, F. Sette, G. van der Laan, *Phys. Rev. Lett.* **1992**, *68*, 1943.

[31] P. Carra, B. T. Thole, M. Altarelli, X. Wang, *Phys. Rev. Lett.* **1993**, *70*, 694.

[32] M. Murugesu, *Nat. Chem.* **2012**, *4*, 347.

[33] C. Wäckerlin, F. Donati, A. Singha, R. Baltic, S. Rusponi, K. Diller, F. Patthey, M. Pivetta, Y. Lan, S. Klyatskaya, M. Ruben, H. Brune, J. Dreiser, *Adv. Mater.* **2016**, *28*, 5195.

[34] G. Cucinotta, M. Perfetti, J. Luzon, M. Etienne, P. -E. Car, A. Caneschi, G. Calvez, K. Bernot, R. Sessoli, *Angew. Chem., Int. Ed.* **2012**, *51*, 1606.

[35] P. Gambardella, S. Rusponi, M. Veronese, S. S. Dhesi, C. Grazioli, A. Dallmeyer, I. Cabria, R. Zeller, P. H. Dederichs, K. Kern, C. Carbone, H. Brune, *Science* **2003**, *300*, 1130.

[36] A. Uldry, F. Vernay, B. Delley, *Phys. Rev. B* **2012**, *85*, 125133.

[37] R. Baltic, M. Pivetta, F. Donati, C. Wäckerlin, A. Singha, J. Dreiser, S. Rusponi, H. Brune, *Nano Lett.* **2016**, *16*, 7610.

[38] Y. -S. Ding, K. -X. Yu, D. Reta, F. Ortu, R. E. P. Winpenny, Y. -Z. Zheng, N. F. Chilton, *Nat. Commun.* **2018**, *9*, 3134.

[39] D. Gatteschi, R. Sessoli, *Angew. Chem., Int. Ed.* **2003**, *42*, 268.

[40] G. Huang, G. Fernandez-Garcia, I. Badiane, M. Camarra, S. Freslon, O. Guillou, C. Daiguebonne, F. Totti, O. Cador, T. Guizouarn, B. L. Guennic, K. Bernot, *Chem. - Eur. J.* **2018**, *24*, 6983.

[41] F. D. Natterer, F. Donati, F. Patthey, H. Brune, *Phys. Rev. Lett.* **2018**, *121*, 027201.

[42] D. Coffey, C. de la Fuente, M. Ciria, D. Serrate, S. Loth, J. I. Arnaudas, *Phys. Chem. Chem. Phys.* **2020**, *22*, 196.

[43] D. Moreno, B. Cirera, S. O. Parreiras, J. I. Urgel, N. Giménez-Agulló, K. Lauwaet, J. M. Gallego, J. R. Galán-Mascarós, J. I. Martínez, P. Ballester, R. Miranda, D. Écija, *Chem. Commun.* **2021**, *57*, 1380.

[44] M. Mannini, F. Bertani, C. Tudisco, L. Malavolti, L. Poggini, K. Misztal, D. Menozzi, A. Motta, E. Otero, P. Ohresser, P. Sainctavit, G. G. Condorelli, E. Dalcanale, R. Sessoli, *Nat. Commun.* **2014**, *5*, 4582.

[45] N. A. Anderson, Q. Zhang, M. Hupalo, R. A. Rosenberg, J. W. Freeland, M. C. Tringides, D. Vaknin, *J. Magn. Magn. Mater.* **2017**, *435*, 212.

[46] Y. Teramura, A. Tanaka, B. T. Thole, T. Jo, *J. Phys. Soc. Jpn.* **1996**, *65*, 3056.

[47] P. Giannozzi, S. Baroni, N. Bonini, M. Calandra, R. Car, C. Cavazzoni, D. Ceresoli, G. L. Chiarotti, M. Cococcioni, I. Dabo, A. Dal Corso, S. de Gironcoli, S. Fabris, G. Fratesi, R. Gebauer, U. Gerstmann, C. Gougoussis, A. Kokalj, M. Lazzeri, L. Martin-Samos, N. Marzari, F. Mauri, R. Mazzarello, S. Paolini, A. Pasquarello, L. Paulatto, C. Sbraccia, S. Scandolo, G. Sclauzero, A. P. Seitsonen, A. Smogunov, P. Umari, R. M. Wentzcovitch, *J. Phys.: Condens. Matter* **2009**, *21*, 395502.

[48] L. A. Constantin, J. P. Perdew, J. M. Pitarke, *Phys. Rev. B* **2009**, *79*, 075126.

[49] J. P. Perdew, A. Ruzsinszky, G. I. Csonka, O. A. Vydrov, G. E. Scuseria, L. A. Constantin, X. Zhou, K. Burke, *Phys. Rev. Lett.* **2008**, *100*, 136406.

[50] G. Kresse, J. Joubert, *Phys. Rev. B* **1999**, *59*, 1758.

[51] J. D. Pack, H. J. Monkhorst, *Phys. Rev. B* **1977**, *16*, 1748.

[52] S. Grimme, J. Antony, S. Ehrlich, H. Krieg, *J. Chem. Phys.* **2010**, *132*, 154104.

[53] M. Methfessel, A. T. Paxton, *Phys. Rev. B* **1989**, *40*, 3616.